Available online at www.sciencedirect.com

ScienceDirect

journal homepage: www.elsevier.com/locate/he

The influence of pre-adsorbed Pt on hydrogen adsorption on B2 FeTi(111)

V. Verdinelli [a], E. Germán [a], P. Jasen [a,*], E. González [a], J.M. Marchetti [a,b]

[a] Departamento de Física, Universidad Nacional del Sur & IFISUR (UNS-CONICET), Av. Alem 1253, 8000 Bahía Blanca, Argentina

[b] Department of Mathematical Science and Technology, Norwegian University of Life Sciences, Drøbakveien 31, Ås 1432, Norway

ARTICLE INFO

Article history:
Received 15 October 2013
Accepted 6 December 2013
Available online 6 January 2014

Keywords:
Hydrogen
Adsorption
B2-FeTi
Platinum
DFT

ABSTRACT

The hydrogen adsorption properties on a Pt covered Fe-terminated B2-FeTi (111) surface are studied using the Density Functional Theory (DFT). The calculations are employed to trace relevant orbital interactions and to discuss the geometric and electronic consequences of incorporating one Pt atom or a Pt monolayer on top of the FeTi surface. The most stable adsorption site is a distorted FCC hollow for one Pt atom and from this location we build the Pt monolayer (ML). The H-adsorption energy is very close among BRIDGE, HCP and FCC hollow sites (~−0.45 eV) being lower for the TOP site (−0.34 eV) in the case of a Pt(111) fcc surface. In the case of a Pt ML/FeTi, the H more stabilized on a BRIDGE site (~−1.13 eV) interacting with both a Pt and Fe atom. We also computed the density of states (DOS) and the overlap population density of states (OPDOS) in order to study the evolution of the chemical bonding after adsorption.

1. Introduction

Hydrogen as an energy carrier is expected to play a crucial role in a future more sustainable society due to the decline of the world's crude oil production. However, one of the key challenges for developing a new clean energy system using hydrogen is associated with its reversible storage, transportation and production [1]. Although several material have been developed for hydrogen storage [2,3], such as metal-organic frameworks (MOFs) [4–7], covalent-organic frameworks (COFs) [8], carbon nanomaterials [9,10], zeolites and mesoporous materials [11], none of them meet the ideal requirements specified by the US Department of Energy (DOE) for H-storage materials. According to the DOE, a 9.0 wt% gravimetric density and 81 g/L volumetric density is the threshold for a sustainable hydrogen storage system [12].

Taking into account both safety and cost, metal/alloy hydrides are good candidates for hydrogen storage [13]. Ivey & Northwood [14] and Sakintuna et al. [15] reviewed many intermetallic alloys that have been studied so far.

Recently, Hout et al. [16] reviewed the recent progress within the experimental methods for preparation of hydrogen storage materials. These authors focus on mechanochemical synthesis method for solid hydrogen storage. The synthesis of innovative materials for energy conversion and storage has received increasing focus during the past decades due to the worlds increasing energy demands and simultaneous needs for environmentally friendly energy technologies [16].

* *Corresponding author*. Tel.: +54 291 4595101x2843; fax: +54 0291 4595142.
E-mail address: pjasen@uns.edu.ar (P. Jasen).

0360-3199/$ – see front matter
http://dx.doi.org/10.1016/j.ijhydene.2013.12.072

Among AB-type intermetallics, FeTi compound is one the most promising hydrogen storage alloys due to its low cost, reversible character for hydriding/dehydriding at near ambient conditions, store capacity of 1.9 wt% hydrogen and kinetics of hydrogen absorption/desorption [17–21]. On the other hand, Reilly & Wishwall [22] observed that this alloy reacts with hydrogen to form two ternary hydrides, i.e., $FeTiH_{\sim 1}$ and $FeTiH_{\sim 2}$ [23,24]. However, the two main drawbacks of this material are: i) the activation process that it requires high heating temperatures ~400 °C and a considerable hydrogen pressure and ii) sensitivity to impurities in the hydrogen gas. This leads to formation of an oxide layer preventing the hydrogen adsorption [18,22,25–30].

As well known, the FeTi hydrogen storage alloy exhibits sluggish rates of H_2 absorption because of stable surface oxide layers. The occurrence of H_2 dissociation is caused by the exchange of electrons between the H_2 molecules and the metal surface [31,32]. Oxide layers on the metal surface hinder the electron exchange and the subsequent H_2 dissociation. This process retards the whole reaction rate of hydrogen adsorption. A nano-structured FeTi alloy (n-FeTi) exhibits remarkably high rates of initial activation and hydrogen absorption compared with those of an untreated FeTi alloy [21]. Edalati et al. [33] shows that FeTi processed by high-pressure torsion (HPT) absorbs and desorbs 1.7 wt% hydrogen at room temperature without activation. The absorption pressure decreases from 2 MPa in the first hydrogenation cycle to 0.7 MPa in the latter cycles.

Several experimental [18,25,34–37] and theoretical [38–42] studies in FeTi showed that the formation of an oxide layer can be prevented by the usage of noble metal coating, such as palladium and platinum.

Bououdina et al. [43] and Heller et al. [44] considered Ni, which is not as expensive as Pd, as coating material. However, the Ni surface is sensitive to CO from air [44]. Moreover, platinum is a well-known electrocatalytic material and is primarily used for fuel-cell applications [2,45–48].

Hydrogen sorption performances of FeTi are very sensitive to the preparation conditions, especially ones that result in contamination of the material with oxygen. The effect of oxygen introduction into FeTi alloy was investigated by Davids et al. [49]. These authors observed that the increase of oxygen content in the alloy results in the decrease of the abundance of the main FeTi phase, together with the increase in the abundance of $Ti_4Fe_2O_{1-x}$. This effect is well-pronounced even at low (0.1–0.2 wt%) oxygen concentrations, as well as when titanium is taken in excess as compared to the stoichiometric Ti:Fe ratio. The introduction of oxygen improved activation performances of the FeTi based material, but decreased its reversible hydrogen absorption capacity.

Solid-oxide-oxygen-ion conducting membrane (SOM) process is a novel, high efficient, low cost, energy-saving, environmentally friendly electrochemical extraction method of metals or alloys. Taking FeTi based hydrogen storage alloy as an example, the authors demonstrated the possibility of SOM process to produce hydrogen storage alloy directly from the oxide; the electrochemical performances of the obtained alloy are also investigated [50].

In this work, a Fe-terminated B2-FeTi (111) slab is considered to study the adsorption of H with a Pt-monolayer (ML). We used the concepts of density of state (DOS) to trace the relevant electronic interaction and overlap population density of states (OPDOS) to characterize the changes in the chemical bonding after hydrogen adsorption.

2. The surface model and the computational method

The inter-metallic B2-FeTi structure is bcc with a lattice parameter $a_0 = 2.976$ Å [51,52]. The unit cell for this structure is shown in Marchetti et al. [41].

The (111) crystallographic plane was selected to perform our study to compare with previous work from Kulkova et al. [39]. The theoretical method and the surface model are considered in the next sections.

2.1. *Computational method*

We performed first-principles calculations based on spin polarized DFT. The Vienna *Ab-initio* Simulation Package (VASP) is used to solve Kohn–Sham equations with periodic boundary conditions and a plane wave basis set [53–55]. Electron-ion interactions are described by ultra-soft pseudopotentials [56], exchange and correlation energies are also calculated using the Revised Perdew–Burke–Ernzerhof form of the spin-polarized generalized gradient approximation (GGA-RPBE), which has been shown to give accurate values for adsorption energies of many molecular species [57]. We used a kinetic energy cutoff of 300 eV for all calculations, which converges total energy to ~1 meV/atom and 0.001 Å for the primitive bulk cell. The Monkhorst–Pack scheme is used for k-point sampling [58]. An equilibrium lattice constant of $a_0 = 2.946$ Å is used and it was obtained with a $7 \times 7 \times 7$ converged mesh within the first Brillouin Zone. The geometry optimization was terminated when the Hellman–Feyman force on each atom was less than 0.02 ev/Å and the energy difference was lower than 10^{-4} eV. The lattice constant is in agreement with experimental XRD data. Bader analysis is used to calculate electronic charges on atoms before and after H adsorption [59].

In the case of one Pt atom in each adsorption site and a Pt ML, the Pt adsorption energy is calculated by:

$$\Delta E_{ads} = [E_{Total}(\mathrm{FeTi}_{slab} + n\mathrm{Pt}) - nE_{Total}(\mathrm{Pt}) - E_{Total}(\mathrm{FeTi}_{slab})]/n \quad (1)$$

where n is the number of Pt atom considered; E_{Total} ($\mathrm{FeTi}_{slab} + n\mathrm{Pt}$) is the total energy of the relaxed Pt/FeTi system; E_{Total} (Pt) is the total energy of an isolated Pt atom and E_{Total} (FeTi_{slab}) is the total energy of the relaxed clean FeTi(111) slab.

After H adsorption, the stabilization of Pt ML/FeTi + H can be better investigated by comparing the adsorption energies of Pt ML/FeTi – starting from the intermetallic surface and molecular hydrogen – given by:

$$\Delta E_{ads} = E_{Total}(\mathrm{H/Pt\ ML/FeTi}) - E_{Total}(\mathrm{Pt\ ML/FeTi}) - \frac{1}{2}E_{Total}(\mathrm{H_2\ molecule}) \quad (2)$$

where E_{Total} (H/Pt ML/FeTi) is the total energy of the relaxed FeTi(111) covered by a Pt ML after H adsorption, system, E_{Total}

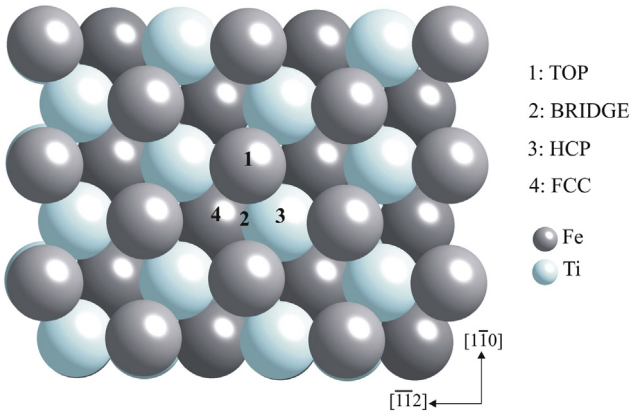

Fig. 1 – Schematic top view of the (111) plane of the B2FeTi alloy. The high symmetry adsorption sites are indicated. The shading colors indicate the different and more inner layers. (For interpretation of the references to color in this figure legend, the reader is referred to the web version of this article.)

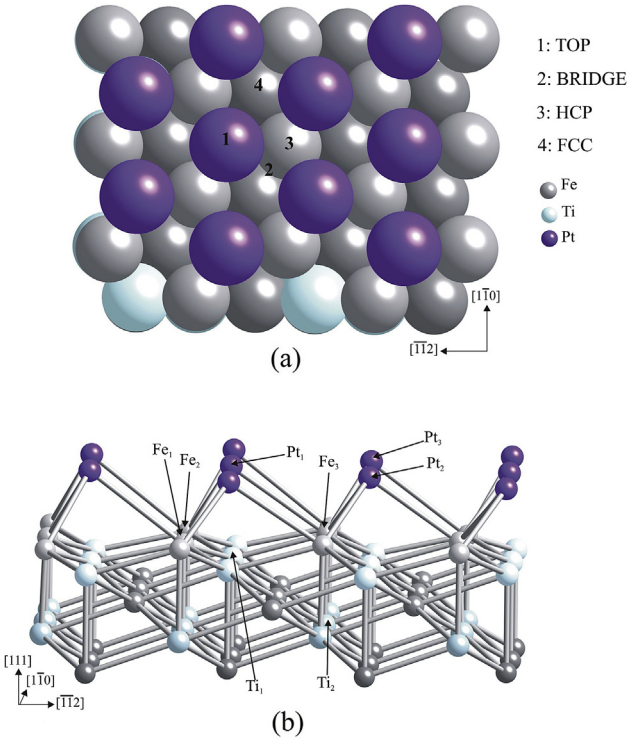

Fig. 3 – (a) Schematic top view of the Pt ML/B2FeTi. The high symmetry sites are also indicated. (b) Schematic lateral view of the Pt ML/B2FeTi where the atoms involved in the OP bonds are indicated. The shading colors indicate the different and more inner layers. (For interpretation of the references to color in this figure legend, the reader is referred to the web version of this article.)

(Pt ML/FeTi) is the total energy of FeTi(111) covered by a Pt ML and E_{Total} (H_2 molecule) is the energy of one isolated H_2 molecule.

2.2. *The surface model*

We represented the (111) plane with a supercell of 48 Fe and 48 Ti atoms. In order to achieve the best compromise between computational time and accuracy of our model, we decided to use a five layers slab separated in the [111]-direction by vacuum regions. The thickness of the vacuum region, corresponding to 4 layers, is enough to avoid interaction between surface images. The thickness of FeTi(111) slab should be such that it approaches the electronic structure of 3D bulk FeTi in its innermost layer. Our slab has two surface-like layers and three inner layers. During the geometry optimization the top three layers of the slab are allowed to relax keeping the bottom two layers fixed in the bulk position. Fig. 1 shows the top view of the clean FeTi(111) surface where the high-symmetry adsorption sites are also indicates: TOP, BRIDGE, HCP and FCC.

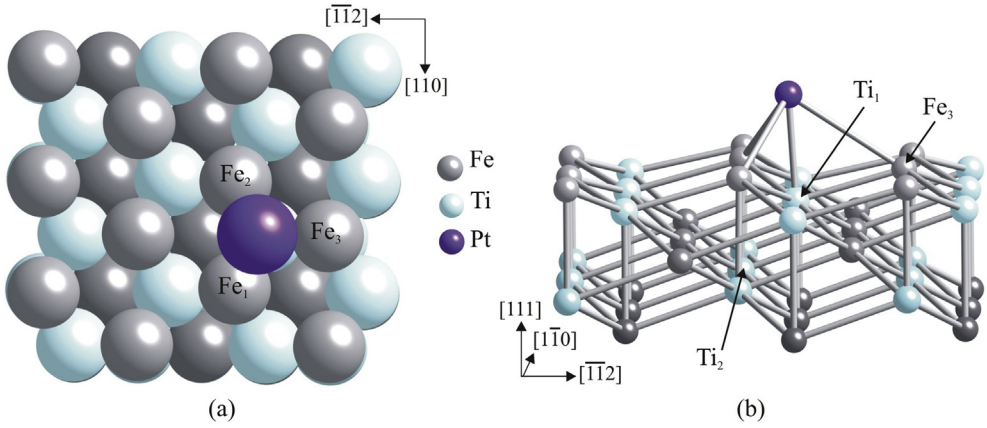

Fig. 2 – Schematic view of the (111) plane from B2FeTi alloy after the Pt adsorption at its minimum energy position: (a) top and (b) lateral. The shading colors indicate the different and more inner layers. (For interpretation of the references to color in this figure legend, the reader is referred to the web version of this article.)

Table 1 – Electron Orbital Occupation, OP and distances for the FeTi (111): clean and Pt atoms adsorbed.

Structure	Electronic Orbital Occupation			Bond type	OP	ΔOP%[a]	Distance (Å)
	s	p	d				
FeTi							
Fe_1	0.80	0.11	8.66	Fe_1–Fe_2	0.000		4.031
Ti_1	0.44	0.11	0.97	Ti_1–Ti_2	0.022		2.969
				Fe_3–Ti_2	0.390		2.402
FeTi + 1 Pt[a]							
Fe_1	0.78	0.28	8.33	Fe_1–Fe_2	0.000	–	4.031
Ti_1	0.44	0.14	1.20	Ti_1–Ti_2	0.017	−22.7	2.968
				Fe_3–Ti_2	0.309	−21.0	2.402
Pt	1.52	2.72	9.74	Pt–Fe_1	0.557	–	2.777
				Pt–Ti_1	0.564	–	2.293
Pt ML/FeTi							
Fe_1	0.71	0.47	6.48	Fe_1–Fe_2[a]	0.000	–	4.195
Ti_1	0.45	0.11	0.98	Ti_1–Ti_2[a]	0.027		2.969
				Fe_3–Ti_2[a]	0.127	−67.5	2.966
Pt_1	1.38	2.24	9.59	Pt_1–Pt_2	0.013	–	4.172
				Pt_1–Fe_1[b]	0.621	11.5[b]	2.641
				Pt_1–Ti_1[b]	0.462	−18.1[b]	2.336

[a] Overlap population percentage change computed referring to the clean surface.
[b] Overlap population percentage change computed referring to the surface with one Pt adsorbed.

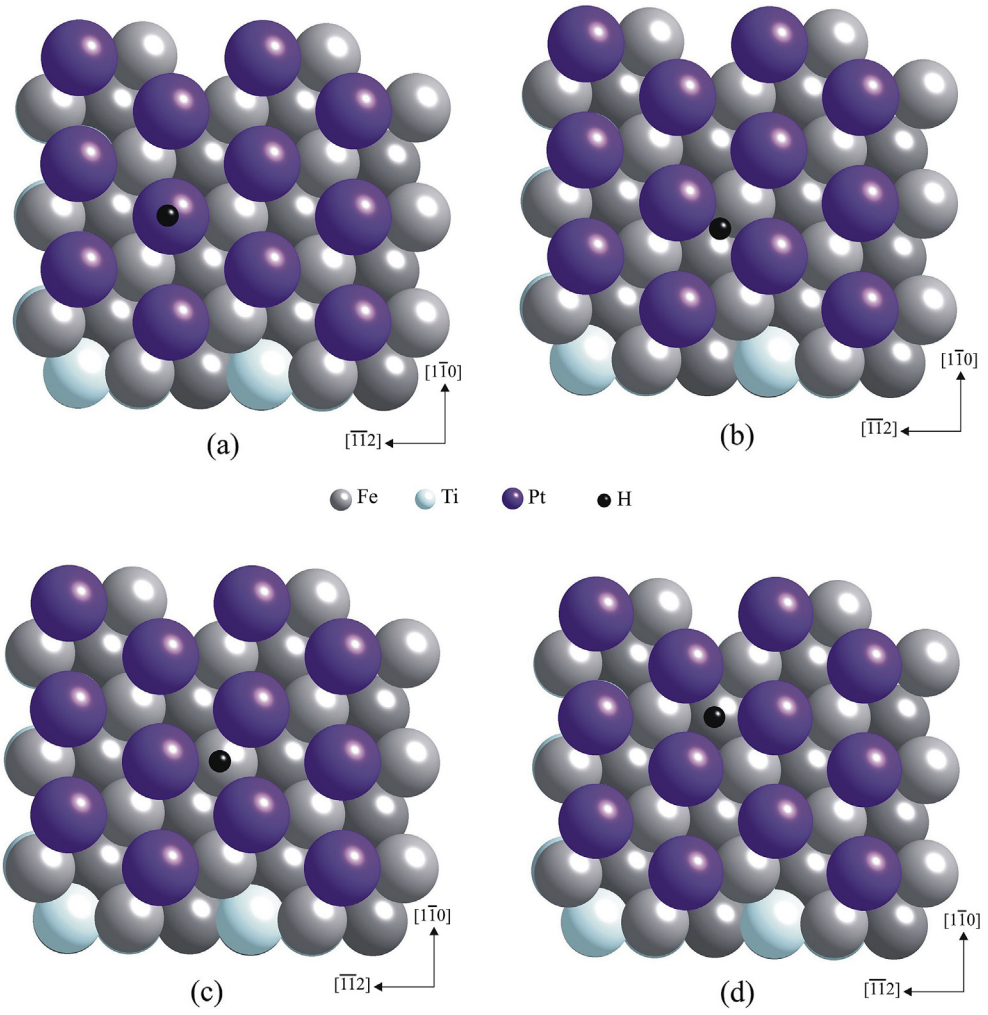

Fig. 4 – Schematic top view of the Pt ML/B2FeTi(111) after H adsorption. In TOP site (a), BRIDGE site (b), FCC (c) and HCP hollow sites (d).

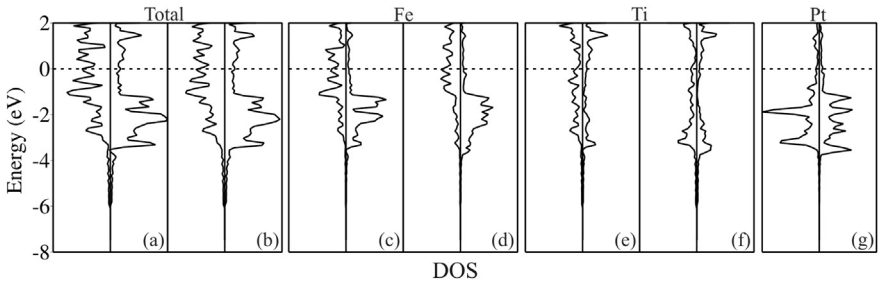

Fig. 5 – DOS curves for the B2-FeTiFe (111) before (a), (c) and (e); and after (b), (d) and (f) with one Pt adsorption. The dashed line placed in Zero eV is the Fermi level. The curves (c)–(f) have 2× magnification.

The Pt ML is build considering the minimum location for a Pt atom and optimizing the geometry. Using a cubic box of 10 Å × 10 Å × 10 Å we obtained a H_2 bond length of 0.751 Å and a binding energy of −4.52 eV in fairly good agreement with experimental values [60].

In order to understand Pt/FeTi and H/Pt ML/FeTi interactions and bonding we used the concept of Density of States (DOS) and the Crystal Orbital Overlap Population (OPDOS) as described by Hoffmann [61]. The SIESTA code is used to compute OPDOS [62,63].

3. Results and discussion

3.1. *Adsorption of a Pt atom and a Pt ML*

The electronic structure of pure FeTi alloy and one Pt adatom on the surface was previously reported [1,27–31]. In the case of one Pt atom, we considered four different high symmetry sites in the FeTi (111) surface: TOP, BRIDGE, FCC and HCP hollow positions.

The adsorption energy for a single Pt atom was −3.71 eV in a distorted hollow position on the B2FeTi surface in agreement with previous calculations of Gonzalez et al. [42]. It can be seen in Fig. 2a, that the HCP hollow has higher coordination and, therefore, becomes favorable for the adsorbed Pt atom. This preference for high coordination of adsorbed atoms and molecules was explained by Légaré [64].

The Pt–Fe and Pt–Ti interaction distances are 2.777 and 2.293 Å respectively. The Fe–Ti distances remain very close to the clean surface where no Pt is present. The DOS plots in Fig. 5 look similar before and after Pt adsorption. The only visible difference is the more hybridized d band on the Fe projection (compare Fig. 5c and d). The OP values in Table 1 indicate the formation of three Pt–Fe bonds and one Pt–Ti bond at expenses of Fe–Ti and Ti–Ti bonds. Although a Pt–Ti bond is developed the effect on the Ti–Ti OP is small.

As mentioned in the introduction, in order to prevent the formation of an oxide layer at the B2-FeTi surface a layer of Pt coating has been suggested [18]. The Pt ML is built matching distorted HCP hollow sites. The minimum Pt ML-surface distance is optimized at 1.067 Å from the surface level (see Fig. 3). The adhesion energy is −3.77 eV that is very close to the adsorption energy in the case of a single Pt atom. The Pt–Fe equilibrium distance is 2.641 Å (somewhat shorter than one Pt case) while the Pt–Ti distance is 2.336 Å, which is larger than one Pt case. This is an indication of higher distortion comparing the case with one Pt atom and a Pt ML.

The Pt–Fe bond is achieved at expenses of Fe_3–Ti_2 OP decrease (about 67.5%) while it's bond length increase to 2.966 Å. Pt–Fe OP value increase about 11% with respect to one Pt atom while the Pt–Ti decrease. The Pt–Pt distances is 4.172 Å and almost no interaction is detected. Fig. 6 shown the OPDOS curves for Fe–Ti, Ti–Ti before an after; and Pt–Fe and Pt–Ti after Pt adsorption.

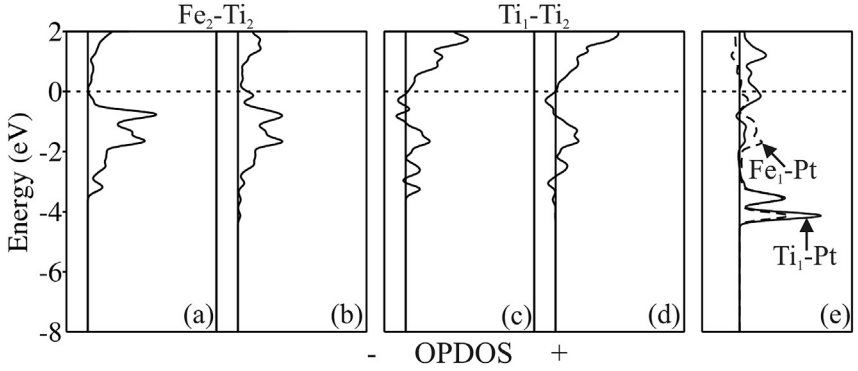

Fig. 6 – OPDOS curves for metal–metal interaction on FeTi (111) before (a) Fe–Ti and (c) Ti–Ti; and after (b) Fe–Ti, (d) Ti–Ti and (e) Pt–Fe and Pt–Ti one Pt adsorption. The dashed line placed in Zero eV is the Fermi level.

Table 2 – Adsorption energies and distances H–Pt, H–Fe and H-surf. for Pt ML/FeTi(111) and Pd(111) FCC surfaces after H adsorption.

	Pt ML/FeTi(111)				Pt(111)			
	TOP	BRI	HCP	FCC	TOP[a]	BRI[b]	HCP[a]	FCC[a]
d_{H-Pt} (Å)	1.70	2.10	2.45	2.47	1.57	n.a.	1.85	1.87
d_{H-Fe} (Å)	–	1.70	2.60	1.68	–	–	–	–
E_{ads} (eV)	−0.34	−1.13	−0.51	−0.97	−0.34	−0.40	−0.45	−0.46
$d_{H\text{-}surf.}$ (Å)	1.70	0.10	−0.10	0.60	1.57	n.a.	0.86.	0.91.

[a] Ref. [65].
[b] Ref. [66].

3.2. *Adsorption of an H atom on the on the Pt ML/FeTi(111)*

After the adsorption of a Pt ML, its effect on the adsorption of hydrogen is also studied. The BRIDGE site is found the most favorable location followed by FCC and HCP hollows and TOP sites (see Table 2). This is due to the large coordination number of the nearest neighbors and minimum repulsion between overlaps charge densities of the metal and the hydrogen atom as was previously reported by Kulkova et al. [39] and Lee et al. [38]. The hydrogen atom is located 0.10 Å above the surface on the BRIDGE site (see Fig. 4b) and in all sites, except TOP, the adsorption energies are more stable than the case of the pure Pt fcc surface [65,66]. The adsorption

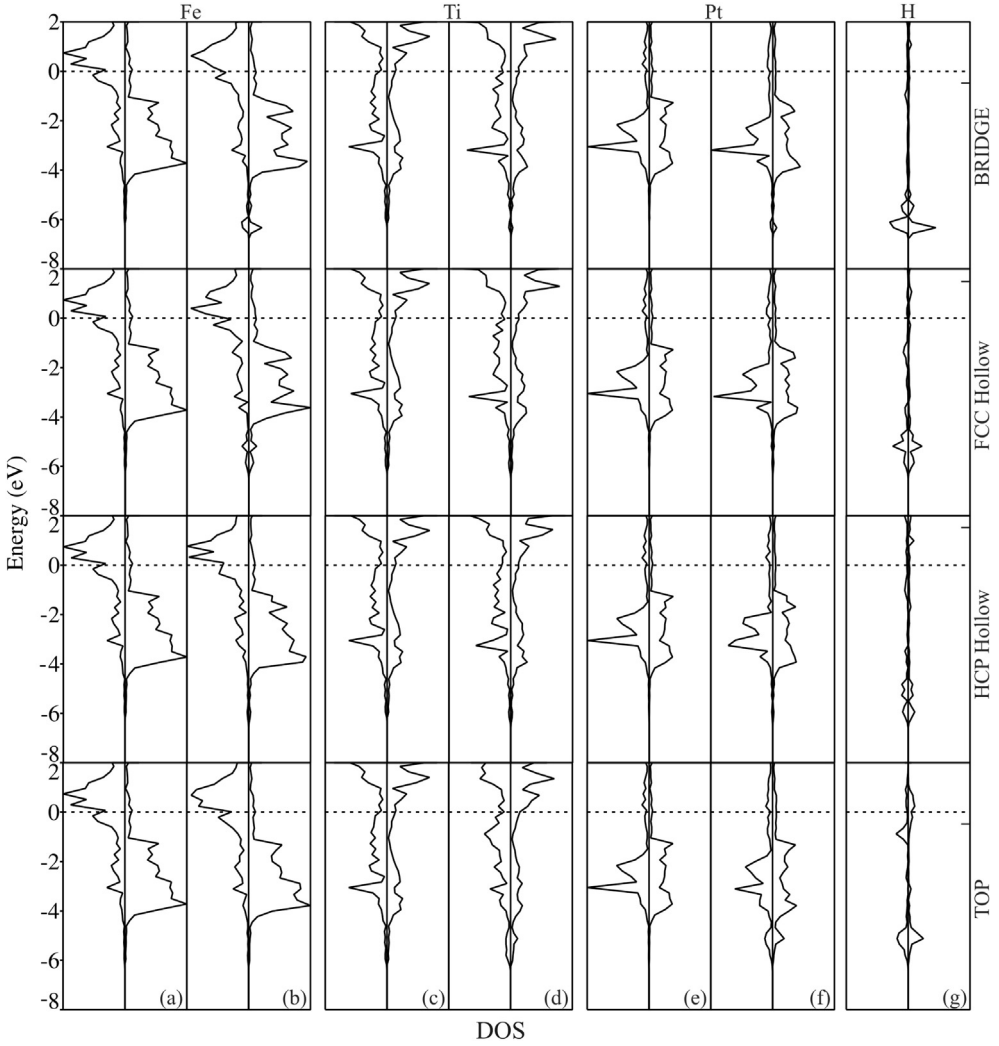

Fig. 7 – DOS curves for the Pt ML/B2FeTi(111) before (a), (c) and (e); and after (b), (d), (f) and (g) H adsorption in all symmetric sites. The dashed line placed in Zero eV is the Fermi level. The curves (a)–(d) and (g) have 2× and 5× magnification respectively. The bar on the left indicates H energy before adsorption.

Table 3 – Electron Orbital Occupation, OP and distances for the Pt ML/FeTi (111) system after Hydrogen adsorption per site.

Structure	Electronic Orbital Occupation			Bond type	OP	ΔOP%
	s	p	d			
H TOP						
Fe	0.71	0.45	6.51	Fe_1–Fe_3[a]	0.000	0.0
Ti	0.45	0.13	0.88	Ti_1–Ti_2[a]	0.026	−3.7
				Fe_3–Ti_2[a]	0.129	+1.6
Pt	1.14	2.37	9.44	Pt_1–Pt_3[b]	0.011	−15.4
				Pt_1–Fe_1[b]	0.566	−8.8
				Pt_1–Ti_1[b]	0.510	+10.4
H	1.29	0.00	0.00	H–Pt_1	0.721	–
H BRI						
Fe	0.59	0.41	6.35	Fe_1–Fe_3[a]	0.000	0.0
Ti	0.45	0.13	0.88	Ti_1–Ti_2[a]	0.027	0.0
				Fe_3–Ti_2[a]	0.126	−0.8
Pt	1.31	2.13	9.54	Pt_1–Pt_2[b]	0.000	−100
				Pt_2–Fe_3[b]	0.442	−28.8
				Pt_1–Ti_1[b]	0.454	−1.7
H	1.21	0.00	0.00	H–Pt_1	0.280	–
				H–Fe_3	0.213	–
H HCP						
Fe	0.68	0.44	6.55	Fe_1–Fe_3[a]	0.000	0.0
Ti	0.45	0.13	0.88	Ti_1–Ti_2[a]	0.027	0.0
				Fe_3–Ti_2[a]	0.130	+2.4
Pt	1.35	2.14	9.55	Pt_1–Pt_3[b]	0.000	−100
				Pt_2–Fe_3[b]	0.632	+1.8
				Pt_1–Ti_1[b]	0.458	−0.9
H	1.29	0.00	0.00	H–Pt_1	0.157	–
				H–Pt_3	0.231	–
				H–Fe_3	0.022	–
H FCC						
Fe	0.57	0.45	6.33	Fe_1–Fe_3[a]	0.000	0.0
Ti	0.45	0.13	0.87	Ti_1–Ti_2[a]	0.028	+3.7
				Fe_3–Ti_2[a]	0.107	−15.7
Pt	1.35	2.11	9.59	Pt_1–Pt_3[b]	0.000	−100
				Pt_2–Fe_3[b]	0.493	−20.6
				Pt_1–Ti_1[b]	0.462	0.0
H	1.28	0.00	0.00	H–Pt_1	0.079	–
				H–Pt_3	0.119	–
				H–Fe_3	0.324	–

[a] Overlap population percentage change computed referring to the clean surface.
[b] Overlap population percentage change computed referring to the surface with Pt pre-adsorbed.

on TOP site present a longer H–Pt distance compared with the Pt(111) surface while the adsorption energy is the same (−0.34 eV).

The Fe–H distance (1.70 Å) is close to that computed by Juan & Hoffman on pure Fe(110) surface [67], in fcc Fe containing a vacancy [68] and on FeTi(110) surface with a one Pt atom pre-adsorbed [41].

The changes in DOS are presented in Fig. 7. In the case of H located in a BRIDGE a small peak at about −6.35 eV indicates H stabilization after adsorption. This interaction can be seen on the Fe and Pt projection. In the cases of hollow sites, the interaction is lower but runs from −6 eV to E_F. The H on TOP present a small peak at −4.94 eV and a projection only on Pt atom as expected. Table 3 presents the changes in metal–metal OP after H adsorption. In the more stable site, the Pt_1–Pt_2 BRIDGE, the Pt_2–Fe_3 OP decrease 28.8% while two H–Pt bonds and one H–Fe bond are formed. The small Pt_1–Pt_2 OP disappear when hydrogen is present. Figs. 8 and 9 show the changes on metal–metal OPDOS curves after H adsorption. Fig. 8 compares Pt_2–Fe_3 and Pt_1–Fe_3 bonds before and after H adsorption. In the BRIDGE adsorption site (see Fig. 8b) the metal–metal bonding at −3.64 eV peak decrease and a bonding peak at −6.35 eV (related to H) is developed. The loose of bonding peak is also present in FCC hollow site but the H–Metal bonding peak is less stabilized at −5.88 eV. Fig. 9 also shows less bonding area between −2 eV and E_F for the Ti_1–Pt_1 bond after H adsorption on the BRIDGE site. Finally Fig. 10 shows the bonding interaction for H–Pt and H–Fe, the bonding peaks locate at lower energies compared with FCC, HCP and is close to TOP.

4. Conclusions

In this work, the influence of pre-adsorbed Pt on hydrogen adsorption on Fe-terminated B2-FeTi (111) is theoretically studied. Our results indicate that the hydrogen is located on a BRIDGE site when a Pt ML covers the FeTi surface. In addition, the OPDOS curves show that the presence of the hydrogen leads to a weakening of metal–metal bonding due to the formation of new bonds between metal and H; being the H–Fe and H–Pt bonds the most important.

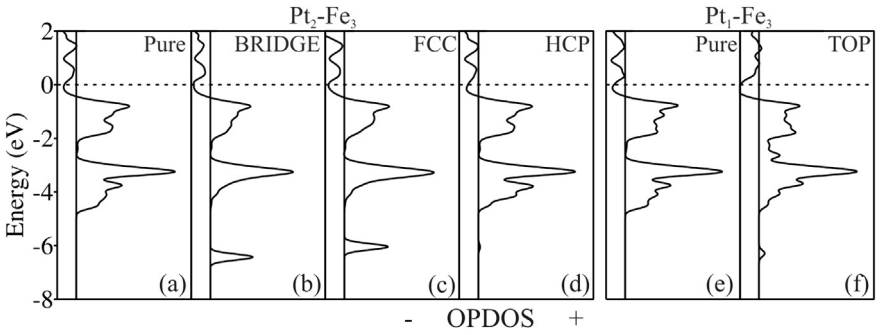

Fig. 8 – OPDOS curves for Pt–Fe bond before (a) and (e) and after (b)–(d) and (g) H adsorption in all symmetric sites. The dashed line placed in Zero eV is the Fermi level. All curves have 4× magnification.

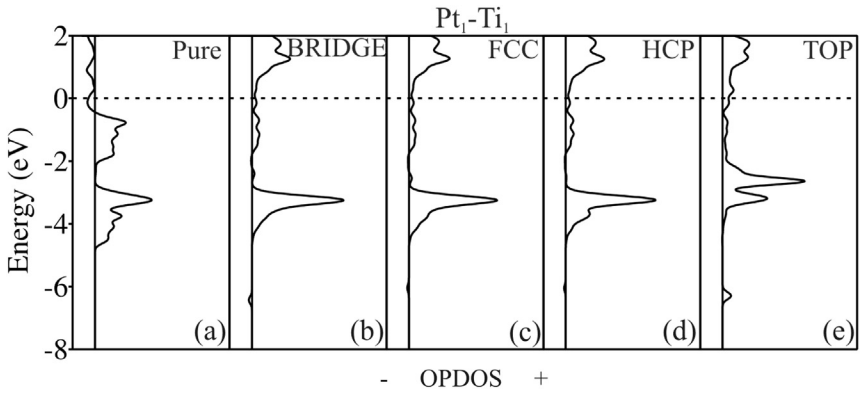

Fig. 9 – OPDOS curves for Pt–Ti bond before (a) and after (b)–(e) H adsorption in all symmetric sites. The dashed line placed in Zero eV is the Fermi level. All curves have 2× magnification.

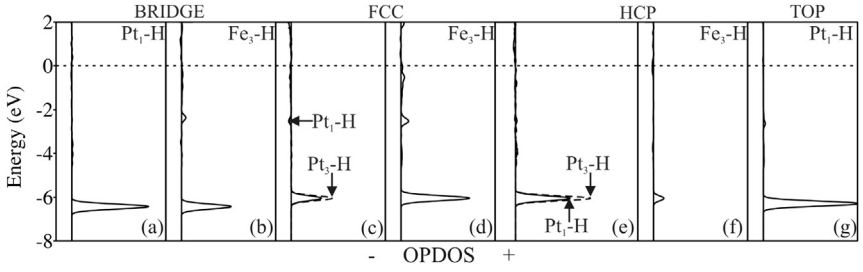

Fig. 10 – OPDOS curves for metal–H bond for all symmetric sites. The dashed line placed in Zero eV is the Fermi level. Curves (a)–(f) have 2× magnification.

Acknowledgements

Our work was supported by ANPCyT through PICT 1770, PIP-CONICET No. 114-200901-00272 and No. 114-200901-00068 Research Grants and SGCyT-UNS, as well as by the Central Research Council of the Norwegian University of Life Sciences (Visiting researcher grant 2012). VV, EG, PJ, EG and JMM are members of CONICET. We kindly acknowledge the useful discussions with Prof. P.V. Messina.

REFERENCES

[1] Izanlou A, Aydinol MK. An ab-initio study of dissociative adsorption of H_2 on FeTi surfaces. Int J Hydrogen Energy 2010;35:1681–92.
[2] Serrano E, Rus G, García-Martínez J. Nanotechnology for sustainable energy. Renew Sust Energy Rev 2009;13(9):2373–84.
[3] David E. An overview of advanced materials for hydrogen storage. J Mater Process Technol 2005;162–163:169–77.
[4] Rowsell JLC, Spencer EC, Eckert J, Howard JAK, Yaghi OM. Gas adsorption sites in a large-pore metal organic framework. Science 2005;309:1350–4.
[5] Sun D, Ma S, Ke Y, Collins DJ, Zhou HC. An interweaving MOF with high hydrogen uptake. J Am Chem Soc 2006;128:3896–7.
[6] Kumar RM, Subramanian V. Interaction of H_2 with fragments of MOF_{-5} and its implications for the design and development of new MOFs: a computational study. Int J Hydrogen Energy 2011;36:10737–47.
[7] Gopalsamy K, Prakash M, Mahesh Kumar R, Subramanian V. Density functional studies on the hydrogen storage capacity of boranes and alanes based cages. Int J Hydrogen Energy 2012;37:9730–41.
[8] Furukawa H, Yaghi OM. Storage of hydrogen, methane, and carbon dioxide in highly porous covalent organic frameworks for clean energy applications. J Am Chem Soc 2009;131:8875–83.
[9] Gundiah G, Govindaraj A, Rajalakshmi N, Dhathathreyan KS, Rao CNR. Hydrogen storage in carbon nanotubes and related materials. J Mater Chem 2003;13:209–13.
[10] Li Y, Zhao D, Wang Y, Xue R, Shen Z, Li X. The mechanism of hydrogen storage in carbon materials. Int J Hydrogen Energy 2007;32:2513–7.
[11] Shepparda DA, Buckley Ce. Hydrogen adsorption on porous silica. Int J Hydrogen Energy 2008;33:1688–92.
[12] Hydrogen, fuel cells & infrastructure technologies program: multi-year research, development, and demonstration plan. U.S. Dept. of Energy; 2005.http://www.eere.energy.gov/hydrogenandfuelcells/mypp/.
[13] Sherif SA, Barbir F, Veziroglu TN. Wind energy and the hydrogen economy review of the technology. Solar Energy 2005;78:647–60.
[14] Ivey DG, Northwood DO. Review, storing energy in metal hydrides: a review of the physical metallurgy. J Mater Sci 1983;18:321–47.
[15] Sakintuna B, Lamari-Darkrim F, Hirscher M. Metal hydride materials for solid hydrogen storage: a review. Int J Hydrogen Energy 2007;32:1121–40.
[16] Hout J, Ravnsbæk, Zhang J, Cuevas F, Latroche M, Jensen TR. Mechanochemical synthesis of hydrogen storage materials. Progress Mat Sci 2013;58:30–75.
[17] Kinaci A, Aydinol MK. Ab initio investigation of FeTi-H system. Int J Hydrogen Energy 2007;32:2466–74.

[18] Kulshreshtha SK, Jayakumar OD, Bhatt KB. Hydriding characteristics of palladium and platinum alloyed FeTi. J Mat Sci 1993;28:4229–33.
[19] Bououdina M, Grant D, Walker G. Review on hydrogen absorbing materials – structure, microstructure, and thermodynamic properties. Int J Hydrogen Energy 2006;31(2):177–82.
[20] Sandrock G. A panoramic overview of hydrogen storage alloys from a gas reaction point of view. J Alloys Compd 1999;293–295:877–88.
[21] Tajima I, Abe M, Uchida H, Hattori M, Miyamoto Y, Haraki T. Hydrogen sorption kinetics of FeTi alloy with nano-structured surface layers. J Alloys Comp 2013;550:S33–5.
[22] Reilly JJ, Wiswall RH. Formation and properties of iron titanium hydride. Inorg Chem 1974;13(1):218–22.
[23] Bowman RC, Attalla A, Tadlock WE. NMR studies of structure and diffusion in metal hydrides. Int J Hydrogen Energy 1977;1(4):421–6.
[24] Endo N, Saitoh H, Machida A, Katayama Y. Formation of BCC TiFe hydride under high hydrogen pressure. Int J Hydrogen Energy 2013;38:6726–9.
[25] Heller EMB, Vredenberg AM, Boerma DO. Oxidation and annealing of thin FeTi layers covered with Pd. Appl Surf Sci 1999;150:227–34.
[26] Inui H, Yamamoto T, Hirota M, Yamaguchi M. Lattice defects introduced during hydrogen absorption-desorption cycles and their effects on P-C characteristics in some intermetallic compounds. J Alloys Compd 2002;330–332:117–24.
[27] Lee JY, Park CN, Pyun SM. The activation process and hydriding kinetics of FeTi. J Less-Common Met 1983;89:163–8.
[28] Schlapbach L, Riesterer T. The activation of FeTi for hydrogen absorption. Appl Phys A 1983;32:169–82.
[29] Schlapbach L, Seiller A, Stucki Y. Surface segregation in FeTi and its catalytic effect on the hydrogenation II: AES and XPS studies. Mater Res Bull 1978;13:1031–7.
[30] Schober T, Wastlake DG. The activation of FeTi for hydrogen storage: a different view. Scripta Metall 1981;15:913–8.
[31] Uchida H. Surface processes of H_2 on rare earth based hydrogen storage alloys with various surface modifications. Int J Hydrogen Energy 1999;24:861–9.
[32] Uchida H, Ohtani Y, Ozawa M, Kawahata T, Suzuki T. Surface processes of H_2 in the initial activation of $LaNi_5$. J Less-Common Met 1991;172–174:983–96.
[33] Edalati K, Matsuda J, Iwaoka H, Toh S, Akiba E, Horita Z. High-pressure torsion of TiFe intermetallics for activation of hydrogen storage at room temperature with heterogeneous nanostructure. Int J Hydrogen Energy 2013;38:4622–7.
[34] Heller EMB, Vredenberg AM, Boerma DO. Hydrogen uptake kinetics of Pd coated FeTi films. Appl Surf Sci 2006;253(3):771–7.
[35] Ma J, Pan V, Wang X, Chen C, Wang Q. Hydrogen storage properties of FeTi 1.3 + x wt% Mm (x = 0.0, 1.5, 3.0, 4.5, 6.0) hydrogen storage alloys. Int J Hydrogen Energy 2000;25:779–82.
[36] Zaluski L, Zaluska A, Tessier P, Ström-Olsen JO, Schulz R. Catalytic effect of Pd on hydrogen absorption in mechanically alloyed Mg_2Ni, $LaNi_5$ and FeTi. J Alloys Compd 1995;217:295–300.
[37] Davids MW, Lototskyy M, Nechaev A, Naidoo Q, Williams M, Klochko Y. Surface modification of TiFe hydrogen storage alloy by metal-organic chemical vapour deposition of palladium. Int J Hydrogen Energy 2011;36:9743–50.
[38] Lee M, Kim JS, Koo YM, Kulkova SE. The adsorption of hydrogen on B2 TiFe surfaces. Int J Hydrogen Energy 2002;27:403–12.
[39] Kulkova SE, Eremeev SV, Egorushkin VE, Kim JS, Oh SY. Hydrogen adsorption on Pd/TiFe (110) surface. Solid State Commun 2003;126(7):405–8.
[40] Kim JS, Oh SY, Lee G, Koo YM, Kukova SE, Egorushkin VE. Theoretical study of the electronic structure and hydrogen adsorption properties in B2-FeTi thin films with Pd coating. Int J Hydrogen Energy 2004;29(1):87–92.
[41] Marchetti JM, González E, Jasen P, Brizuela G, Juan A. Interaction of hydrogen and platinum over a B2-FeTi (110) slab. Int J Hydrogen Energy 2011;36:9037–44.
[42] González E, Jasen P, Marchetti JM, Brizuela G, Juan A. Density functional and bonding study of hydrogen and platinum adsorption on B2-FeTi (111) slab. Int J Hydrogen Energy 2012;37:2661–8.
[43] Bououdina M, Fruchart D, Jacquet S, Pontonnier L, Soubeyroux JL. Effect of nickel alloying by using ball milling on the hydrogen absorption properties of TiFe. Int J Hydrogen Energy 1999;24(9):885–90.
[44] Heller EMB, Vredenberg AM, Boerma DO. H uptake kinetics of FeTi films coated with Ni. Appl Surf Sci 2006;253(3):1150–3.
[45] Ford DC, Xu Y, Mavrikakis M. Atomic and molecular adsorption on Pt(111). Surf Sci 2005;587(3):159–74.
[46] Cortright RD, Davda RR, Dumesic JA. Hydrogen from catalytic reforming of biomass-derived hydrocarbons in liquid water. Nature 2002;418(6901):964–7.
[47] Dunn S. Hydrogen future: towards a sustainable energy system. Int J Hydrogen Energy 2002;27(3):235–64.
[48] Barreto L, Makihira A, Riahi K. The hydrogen economy in the 21st century: a sustainable development scenario. Int J Hydrogen Energy 2003;28(3):267–84.
[49] Davids MW, Lototskyy M. Influence of oxygen introduced in ToFe-based hydride forming alloy on its morphology, structural and hydrogen sorption properties. Int J Hydrogen Energy 2012;37:18155–62.
[50] Ye XS, Lu XG, Li CH, Ding WZ, Zou XL, Gao YH, et al. Preparation of Ti-Fe based hydrogen storage alloy by SOM method. Int J Hydrogen Energy 2011;36:4573.
[51] Villars P, Calvert LD. Pearson's handbook of crystallographic data for intermetallic phases. Metals Park, OH: American Society for Metals; 1985.
[52] Brandes EA, Brook GB. Smithells metals reference book. 7th ed. London: Butterworth-Heinemann; 1992.
[53] Kresse G, Hafner J. Ab initio molecular dynamics for liquid metals. Phys Rev B 1993;47:558–61.
[54] Kresse G, Furthmüller J. Efficient iterative schemes for *ab initio* total-energy calculations using a plane-wave basis set. Phys Rev B 1996;54:11169–86.
[55] Kresse G, Furthmüller J. Efficiency of ab-initio total energy calculations for metals and semiconductors using a plane-wave basis set. Comput Mater Sci 1996;6:15–50.
[56] Vanderbilt D. Soft self-consistent pseudopotentials in a generalized eigenvalue formalism. Phys Rev B 1990;41:7892–5.
[57] Hammer B, Hansen LB, Nørskov JK. Improved adsorption energetics within density-functional theory using revised Perdew-Burke-Ernzerhof functionals. Phys Rev B 1999;59:7413–21.
[58] Monkhorst HJ, Pack JD. Special points for Brillouin-zone integrations. Phys Rev B 1976;13:5188–92.
[59] Bader RFW. Atoms in molecules: a quantum theory. Oxford: Oxford University Press; 1990.
[60] Huber KP, Hertzberg G. Molecular spectra and molecular structure IV: constants of diatomic molecules. New York: Van Norstrand Reinhold; 1979.
[61] Hoffmann R. Solid & surface: a chemist's view of bonding in extended structures. New York: Wiley-VCH; 1989.

[62] Ordejón P, Artacho E, Soler JM. Self-consistent order-*N* density-functional calculations for very large systems. Phys Rev B 1996;53:R10441–4.
[63] Soler JM, Artacho E, Gale JD, Garcia A, Junquera J, Ordejón P, et al. The SIESTA method for ab initio order-N materials simulation. J Phys Condes Matter 2002;14:2745–79.
[64] Légaré P. A theoretical study of H surface and subsurface species on Pt (111). Surf Sci 2004;559:169–78.
[65] Saad F, Zemirli M, Benakki M, Bouarab S. Ab-initio study of the co-adsorption of Li and H on Pt(001), Pt(110) and Pt(111) surfaces. Phys B 2012;407:698–704.
[66] Källén G, Washnström G. Quantum treatment of H adsorbed on a Pt(111) surface. Phys Rev B 2001;65. 033406 (1–4).
[67] Juan A, Hoffmann. Hydrogen on the Fe (110) surface and near bulk bcc Fe vacancies. A comparative bonding study. Surf Sci 1999;421:1–16.
[68] Simonetti S, Rey Saravia D, Brizuela G, Juan A. The effects of a hydrogen pair in the electronic structure of the FCC iron containing a vacancy. Int J Hydrogen Energy 2010;35:5957–62.